

# Advancing Residual Learning towards Powerful Deep Spiking Neural Networks

Yifan Hu, Yujie Wu, Lei Deng and Guoqi Li

Department of Precision Instrument, Tsinghua University

## Abstract

Despite the rapid progress of neuromorphic computing, inadequate capacity and insufficient representation power of spiking neural networks (SNNs) severely restrict their application scope in practice. Residual learning and shortcuts have been evidenced as an important approach for training deep neural networks, but rarely did previous work assess their applicability to the characteristics of spike-based communication and spatiotemporal dynamics. In this paper, we first identify that this negligence leads to impeded information flow and accompanying degradation problem in previous residual SNNs. Then we propose a novel SNN-oriented residual block, MS-ResNet, which is able to significantly extend the depth of directly trained SNNs, e.g. up to 482 layers on CIFAR-10 and 104 layers on ImageNet, without observing any slight degradation problem. We validate the effectiveness of MS-ResNet on both frame-based and neuromorphic datasets, and MS-ResNet104 achieves a superior result of 76.02% accuracy on ImageNet, the first time in the domain of directly trained SNNs. Great energy efficiency is also observed that on average only one spike per neuron is needed to classify an input sample. We believe our powerful and scalable models will provide a strong support for further exploration of SNNs.

## 1 Introduction

Spiking neural networks are a typical kind of brain-inspired models with their unique features of rich neuronal dynamics and diverse coding schemes. Different from traditional artificial neural networks (ANNs), SNNs are capable of encoding information in spatiotemporal dynamics and using asynchronous binary spiking activities for event-driven communication. Recent progress in neuromorphic computing has demonstrated their great energy efficiency [Roy *et al.*, 2019]. Theoretically, SNNs are at least as computationally powerful as ANNs and the universal approximation theorem also applies to SNNs [Maass, 1997], so it is not surprising that SNNs have been reported in various domains, such as image

classification, object detection and tracking, speech recognition, light-flow estimation and so forth. However, the status quo of deficiency in powerful SNN models seriously limits their capabilities for complex tasks in practice.

Conversion from a pre-trained model and surrogate gradient-based direct training are two mainstream approaches for obtaining an SNN. The conversion method is free of the dilemma caused by the non-differentiable spiking activation function and can implement the inference of deep SNNs with tens or even hundreds of layers [Sengupta *et al.*, 2019; Han *et al.*, 2020; Hu *et al.*, 2018; Stöckl and Maass, 2021]. Although comparable accuracy to the pre-trained models can be achieved, the method treats SNNs more as an alternative expression of ANNs, and hundreds of time steps are usually required to achieve a satisfying conversion loss. It thereby fails to achieve low-latency computation in practical applications. The latter method utilizes a surrogate gradient function to enable backpropagation through time (BPTT) in the direct training of SNNs. The networks learn to encode information effectively and consequently need much fewer time steps than the conversion ones. In addition, they are inherently more suited for processing spatiotemporal data from the emerging AER-based (address-event-representation) sensors to which the pretrained ANNs and converted SNNs are not applicable.

Unfortunately, one prominent problem of the directly trained SNNs lies in the limited scale of models. Earlier works mainly focus on shallow structures and simple tasks such as MNIST. Inspired from the representation power of deep ANNs, recent works have gradually evolved from fully-connected networks to convolutional networks to more advanced ResNet, for example Zheng *et al.* report the successful training of spiking ResNet-34 on ImageNet. However, the plain transplantation of canonical ResNet, a way almost all previous works have adopted, does not work appropriately for the training of SNNs and the symptom will manifest itself in our depth-analysis experiments as an accuracy drop on both the training and test sets as the network deepens, which is named the degradation problem. As a result, building a deeper SNN still appears to be arduous and fruitless.

We summarize our major contributions in this work as follows:

- We report the degradation problem when applying vanilla ResNet in deep SNN training, and reveal the implicit unavailing residual representation and unstable

gradient norm which prevent the structure from going deeper.

- We design a novel alternative residual block, MS-ResNet, which enables us to significantly extend the depth of directly trained SNNs, e.g., up to 482 layers on CIFAR-10 and 104 layers on ImageNet, without slight degradation problem.
- We evaluate the effectiveness of our methods on various datasets and obtain accuracy results which are, to the best of our knowledge, the state of the art in directly trained SNNs and competitive to the conversion methods via extremely fewer time steps. Along with the sparse spiking activities, great energy efficiency is also validated and it achieves up to 24x energy saving on event streams.

## 2 Related Works

### 2.1 SNN Training Algorithms

There are two main routines to train a high-accuracy SNN model. The first is the conversion method. Its basic idea is that the activation values in a ReLU-based ANN can be approximated by the average firing rates of an SNN under the rate coding scheme. After training an ANN with certain structural restrictions, it is feasible to convert the pre-trained ANN into its spiking counterpart. Conversion-based SNNs maintain the smallest gap with ANNs in terms of accuracy and can be generalized to large-scale structures, such as VGG and ResNet [Rueckauer *et al.*, 2017; Stöckl and Maass, 2021]. However, the method also has its inherent defects. An accuracy gap will be caused by the constraints on ANN models and a long simulation with hundreds or thousands of time steps is required to complete an inference, which leads to extra delay and energy consumption.

The second routine is to utilize a surrogate gradient function, which constitutes a continuous relaxation of the non-smooth spiking to enable standard BP or BPTT for training an SNN from scratch. Direct training algorithms appear to be diverse in the selection of gradient functions and coding schemes [Neftci *et al.*, 2019]. These works have a great advantage in the number of time steps and can be particularly appealing for the implementation on power-efficient neuromorphic hardware. Moreover, directly trained SNNs often take neuronal dynamics into further consideration during training and the capability for processing spatiotemporal event-stream data is always regarded as a critical measurement. Unfortunately, their shallow structures obstruct further exploration on large-scale and complex tasks. Zheng *et al.* propose TDBN to alleviate the depth dilemma and firstly obtain directly trained ResNet-34/50, but their results are not satisfying enough compared to the converted SNNs or ANNs. We also notice a contemporaneous work that looks into deep residual SNNs [Fang *et al.*, 2021] by adding element-wise operations into two spiking branches within a Res-block. Their method is similar but orthogonal to ours.

### 2.2 Residual Learning

Theoretical and empirical evidences indicate that the depth of neural networks is crucial for their success, but the train-

ing becomes more difficult as the depth increases [Srivastava *et al.*, 2015]. Starting with ResNet [He *et al.*, 2016a; He *et al.*, 2016b], the shortcut connection is introduced as an additional branch for an unimpeded flow of both information and its gradient. It is widely adopted in later works, such as DenseNet, Inception-ResNet, and Transformer. One explanation for its superiority is that ResNet works as an implicit ensemble of numerous shallower networks [Veit *et al.*, 2016]. In addition, via the perspective of dynamical mean field theory, ResNet is proved to achieve dynamical isometry in a universal way [Tarnowski *et al.*, 2019]. Obviously, residual learning has gone beyond the ResNet structure and becomes a key component in network structures. It has been utilized in the converted SNNs but remains challenging in the directly trained SNNs. In our work, the drawbacks of adopting canonical ResNet in SNNs are revealed and an improved spiking residual block is proposed.

## 3 Preliminaries and Motivation

### 3.1 Preliminaries of SNNs

The basic differences between an SNN and an ANN originate from their primary computing element, i.e., the neuron. In ANNs, a biological neuron is abstracted as an information aggregation unit with a nonlinear transformation. Meanwhile in SNNs, membrane potential dynamics and spiking communication scheme are more closely mimicked. In this work, we select the iterative LIF model proposed by Wu *et al.*, which is formulated as

$$u_i^t = \tau_{mem} \cdot u_i^{t-1} + \sum_{j=1}^n w_{ij} o_j^t, \quad (1)$$

$$o_i^t = g(u_i^t) = \begin{cases} 1, & u_i^t - V_{th} \geq 0 \\ 0, & u_i^t - V_{th} < 0 \end{cases}, \quad (2)$$

where  $u_i^t$  is the membrane potential of the  $i$ -th neuron in a layer at time step  $t$ ,  $\tau_{mem}$  is a decay factor for leakage and the synaptic input is the weighted sum of output spikes from the previous layer.  $g(\cdot)$  describes the firing activity controlled by the threshold  $V_{th}$  and  $u_i^t$  will be subsequently reset to  $V_{reset}$  once a spike fires. The surrogate gradient is defined as

$$\frac{\partial o_i^t}{\partial u_i^t} = \frac{1}{a} \text{sign} \left( |u_i^t - V_{th}| \leq \frac{a}{2} \right). \quad (3)$$

The coefficient  $a$  is introduced to ensure that the integral of the function is 1. In this way, BPTT can be carried out along with the autograd framework of current deep learning libraries.

For computer vision tasks, a stacking of  $\{\text{Conv-BN-Nonlinearity}\}$  is a universal architecture which follows the primary philosophy of VGG network, and is referred to as PlainNet in this work. We adopt TDBN technique [Zheng *et al.*, 2021] as BN in our spiking models and formulate it as

$$u_i^t = \tau_{mem} u_i^{t-1} + TDBN(I_i^t, \mu_{c_i}, \sigma_{c_i}^2, V_{th}), \quad (4)$$

where  $\mu_{c_i}, \sigma_{c_i}^2$  are channel-wise mean and variation calculated per-dimension over a mini-batch of the sequential input  $\{I_i^t = \sum_{j=1}^n w_{ij} o_j^t | t = 1, \dots, T\}$ .

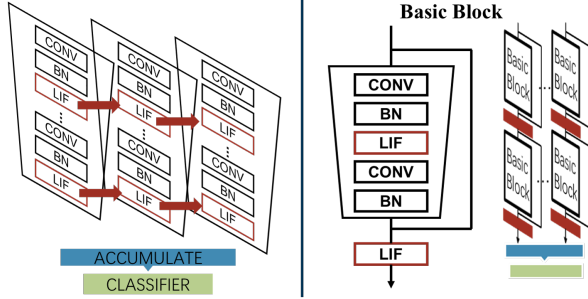


Figure 1: Spiking PlainNet and vanilla ResNet in SNNs.

A shortcut connection can be inserted into PlainNet and turns it into its residual counterpart, which can be written as

$$o^{l+1} = LIF \left( \mathcal{F} \left( o^l; \mathbf{W}^{l+1} \right) + o^l \right), \quad (5)$$

where  $\mathcal{F}(\cdot)$  represents the group of functions in a residual path with  $\mathbf{W}^{l+1}$  as its parameters,  $o^l$  is the spiking train output vector over a simulation period  $T$  and  $l, l+1$  represent the layer index. The direct transplantation of a residual block from non-spiking ResNet is shown in Figure 1, which is a conventional practice in previous works [Zheng *et al.*, 2021; Hu *et al.*, 2018].

### 3.2 The Degradation Problem in SNNs

The most straightforward way of training higher quality models is by increasing their size, especially given the availability of a large amount of labeled training data [Szegedy *et al.*, 2015]. However, directly deepening network has never seemed to be a trustworthy approach to more satisfying accuracy in the field of SNNs.

We would firstly explore the extend to which the BN technique and shortcut connections have helped with the scalability of spiking models. Therefore, we conduct an experiment on CIFAR-10 [Krizhevsky *et al.*, 2009] with depth as the only variable. It should be noted that our focus is on the response of a network to its depth and potential degradation problem rather than pushing the state-of-the-art results, so we use deep but relatively narrow architectures as in Table 1.

Table 2 shows the results of depth analysis. The accuracy of PlainNet with BN begins to drop at the depth of 14 layers, and surprisingly the adoption of shortcut connections will just shift the peak to 20 layers. Despite a gentler slope after the peak, severe accuracy loss still occurs in spiking ResNet when it reaches 56 layers. The degradation problem does exist in spite of the adoption of BN and shortcut connections, indicating that the direct transplantation of ResNet to SNNs does not work appropriately and making building sufficiently deep and powerful SNN models a nontrivial task.

Interestingly, we have noticed that the degradation problem could be alleviated within the depth of 56 layers when we remove the spiking activation functions  $LIF(\cdot)$  between residual blocks and maintain those in the residual paths as nonlinearity. Based on this observation, we mainly identify the crux of degradation as the interblock  $LIF(\cdot)$ , and will provide further insight into it along with our proposed architecture in the next section.

Layers	1 + 2n	2n	2n
Output Size	32x32	16x16	8x8
Channels	16	32	64

Table 1: The structure for depth analysis on CIFAR-10.

Depth	8	14	20	32	44	56
PlainNet	81.1	<b>85.2</b>	83.7	76.4	59.5	N/A
ResNet	81.5	85.9	<b>86.7</b>	85.4	84.6	72.4
W/O $LIF(\cdot)$	80.0	86.9	88.2	88.8	89.4	<b>90.0</b>
<b>Our work</b>	82.0	87.4	88.4	89.7	90.0	<b>90.4</b>

Table 2: Depth analysis on CIFAR-10.

## 4 Spiking Residual Blocks

In this section, we will try to explain why the interblock  $LIF(\cdot)$  obstructs the applicability of vanilla ResNet in the specifics of SNNs' characteristics, introduce the corresponding superiority of our model as well as some other concerns about the new design. The advantages of our model are three-fold:

- An unimpeded inference flow which can avoid unavailable residual expression and imbalanced workload.
- Achieving block dynamical isometry which is an important metric to avoid gradient vanishing or explosion problem.
- Primary energy-efficient features which are intentionally maintained and will suit for further implementation on neuromorphic hardware.

The spiking residual block we proposed is illustrated in Figure 2. The interlayer  $LIF(\cdot)$  is removed to construct a shortcut that goes throughout the whole network and mainly deals with the confluences of different residual paths. Meanwhile an additional  $LIF(\cdot)$  is placed at the top of the residual path to convert messages into sparse spikes and send them to subsequent neurons. What flows in the shortcut is conceptually closer to membrane potentials rather than spiking activities in the original structure. So we name the new structure as the Membrane-Shortcut ResNet (MS-ResNet) to emphasize the change in the shortcut.

### 4.1 Residual Representation and Workload Balance at Inference

Basically, in residual learning we would like a residual path to learn the relatively small perturbation with reference to the identity mapping and these perturbations accumulate into an optimal transformation as the network deepens.

In vanilla spiking ResNet, an identity mapping can be easily achieved by the block when we set the threshold  $V_{th}$  smaller than 1 (e.g. 0.5) and the residual part is close to 0,  $o_i^{l+1} = LIF(\mathcal{F}(o^l) + o_i^l) \approx LIF(o_i^l) = g(o_i^l) = o_i^l$ , i.e. a spike in the shortcut can always induce firing at the next layer and an inactive neuron will not activate its subsequent one. However, what if we want to change a neuron's firing state af-

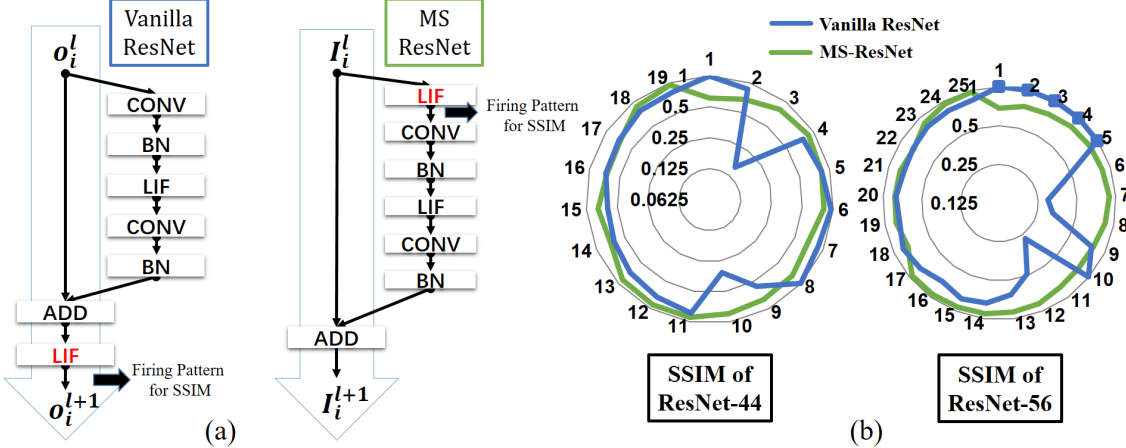


Figure 2: (a) Basic blocks in vanilla spiking ResNet and MS-ResNet. (b) The SSIM radar chart of ResNet-44 and ResNet-56.

ter receiving messages from a residual path, i.e.  $(o_i^{t,l}, o_i^{t,l+1}) \in S = \{s_i = (o_i^{t,l}, o_i^{t,l+1}) \mid o_i^{t,l} + o_i^{t,l+1} = 1, o_i^t \in \{0, 1\}\}$ ?

The probability of a successful change to the firing state can be decomposed into two conditions, which can be written as

$$\begin{aligned} P(s_i \in S) &= P(s_i = (0, 1)) + P(s_i = (1, 0)) \\ &= P(\mathcal{F}(\mathbf{o}^{t,l}) + o_i^{t,l} > V_{th} \mid o_i^{t,l} = 0) P(o_i^{t,l} = 0) \\ &\quad + P(\mathcal{F}(\mathbf{o}^{t,l}) + o_i^{t,l} < V_{th} \mid o_i^{t,l} = 1) P(o_i^{t,l} = 1), \end{aligned} \quad (6)$$

where the part of decayed membrane potential is omitted here for simplicity. Assume the synaptic input the interblock  $LIF(\cdot)$  receives is normally distributed  $\mathcal{F}(\mathbf{o}^{t,l}) \sim \mathcal{N}(0, \sigma_x^2)$ . With variance  $\sigma_x = V_{th} = 0.5$  (a representative value adopted in Zheng *et al.*), we have  $P(\mathcal{F}(\mathbf{o}^{t,l}) > V_{th} \mid o_i^{t,l} = 0) = P(\mathcal{F}(\mathbf{o}^{t,l}) + 1 < V_{th} \mid o_i^{t,l} = 1) = \int_{-\infty}^1 \frac{1}{\sqrt{2\pi}} e^{-\frac{x^2}{2}} \approx 16\%$  and  $P(s_i \in S) \approx 16\%$ . Especially, for the majority of neurons of which the activation states do not change between  $l$  and  $l+1$  layers we have

$$\begin{aligned} o_i^{t,l+2} &= LIF(\mathcal{F}(\mathbf{o}^{t,l+1}; \mathbf{W}^{l+2}) + o_i^{t,l+1}) \\ &= LIF(\mathcal{F}(\mathbf{o}^{t,l}; \mathbf{W}^{l+2}) + o_i^{t,l}), \end{aligned} \quad (7)$$

which indicates that the residual path of  $l+1$ -th layer does not contribute to the overall capacity of the network at timestep  $t$  and we consider it as an unavailing residual representation.

A straightforward solution could be increase the variance of the synaptic input  $\sigma_x^2$ , which leads to higher probability of changing neuronal states and less unavailing residual paths. However, this solution can never completely prevent unavailing residual representation and a significant increase in the importance of residual paths disobeys the perturbation learning rule of ResNet.

While for MS-ResNet, the identity mapping is not constrained to the discrete spiking activity and the small residual

representation can always be accumulated as

$$\begin{aligned} \mathbf{I}^{t,l+2} &= \mathbf{I}^{t,l} + \sum_{k=l}^{l+1} \mathcal{F}(LIF(\mathbf{I}^{t,k}); \mathbf{W}^{k+1}) \\ &= \mathbf{I}^{t,1} + \sum_{k=1}^{l+1} \mathcal{F}(LIF(\mathbf{I}^{t,k}); \mathbf{W}^{k+1}), \end{aligned} \quad (8)$$

where  $\mathbf{I}^{t,l}$  represents the synaptic input vector of  $l$ -th layer. The removing of the interblock  $LIF(\cdot)$  provides a clean path for the information flow and the confluences of residual paths will not be judged by an unnecessary gating function, so unavailing residual representation will not occur regardless of whether the firing state actually changes.

To give a more intuitive verification about how firing patterns may change along with residual blocks of different layers, we adopt structural similarity index measure (SSIM) to quantify the similarity between them, which can be formulated as

$$SSIM(x, y) = \frac{(2\mu_x\mu_y + C_1)(2\sigma_{xy} + C_2)}{(\mu_x^2 + \mu_y^2 + C_1)(\sigma_x^2 + \sigma_y^2 + C_2)}, \quad (9)$$

with  $\mu_x, \sigma_x^2, \mu_y, \sigma_y^2$  the mean and variance of image  $x$  and  $y$ ,  $\sigma_{xy}$  the covariance of  $x$  and  $y$ , and  $C_1, C_2$  two stabilization constants. The pixel-value of an image is defined as the firing rate of a neuron and the sampling point is illustrated in Figure 2. The value of SSIM ranges from -1 and +1, and only equals +1 if the two images are identical.

If the firing pattern changes uniformly between layers, it will appear as a circle in the radar chart of Figure 2. Although a strict circle does not seem to be applicable for the whole neural network due to downsampling layers, our MS-ResNet has shown a rounder curve than vanilla spiking ResNet. Especially, there are 5 layers with an SSIM value of +1 in vanilla ResNet-56, which implies that the firing patterns do not change when information flows through the residual blocks and that these layers fail to help with feature extraction. Consequently, a following layer needs to compensate for the inaction of preceding layers, and it is shown as an ensuing dramatic information change at 6-th layer. The workload

of the whole network is unbalanced especially when it comes to the training of deep networks, which undoubtedly reflects the irrationality of the spiking ResNet, while MS-ResNet has effectively alleviated this unbalance.

## 4.2 Gradient Evolvement at Backpropagation

Dynamical isometry, the equilibration of singular values of the input-output Jacobian matrix, has been developed in recent years as a theoretical explanation of well-behaved neural networks. In this subsection, we analyze with block dynamical isometry framework [Chen *et al.*, 2020] that MS-ResNet can achieve gradient norm equality while the vanilla spiking ResNet cannot.

Without loss of generality, a neural network can be viewed as a serial of blocks:

$$f(x_0) = f_{\theta^L}^L \circ f_{\theta^{L-1}}^{L-1} \circ \cdots \circ f_{\theta^1}^1(x_0), \quad (10)$$

where  $\theta^i$  is the parameter matrix of the  $i$ -th layer. For the sake of simplicity, we denote  $\frac{\partial f^j}{\partial f^{j-1}} = J_j$ . Let  $\phi(J)$  be the expectation of  $tr(J)$  and  $\varphi(J)$  be  $\phi(J^2) - \phi(J)^2$ .

**Definition 1** (Block Dynamical Isometry). *Consider a neural network that can be represented as Equation 10 and the  $j$ -th block's Jacobian matrix is denoted as  $J_j$ . If  $\forall j$ ,  $\phi(J_j J_j^T) \approx 1$  and  $\varphi(J_j J_j^T) \approx 0$ , the network achieves block dynamical isometry [Chen *et al.*, 2020].*

**Lemma 1.** *Assuming that for each of  $L$  sequential blocks in a neural network, we have  $\phi(J_i J_i^T) = \omega + \tau \phi(\widetilde{J}_i \widetilde{J}_i^T)$  where  $J_i$  is its Jacobian matrix. Given  $\lambda \in \mathbb{N}^+ < L$ , if  $C_L^\lambda (1 - \omega)^\lambda$  and  $C_L^\lambda \tau^\lambda$  are small enough, the network would be as stable as a  $\lambda$ -layer network when both networks have  $\forall i, \phi(J_i J_i^T) \approx 1$  [Chen *et al.*, 2020].*

Based on Definition 1 and Lemma 1, we can judge whether a network can achieve gradient norm equality in the specifics of SNNs.

**Proposition 1.** *Assuming both two neural networks consisting of  $L$  sequential blocks, the vanilla spiking ResNet does not achieve block dynamical isometry while MS-ResNet could be as stable as a  $\lambda$ -layer network which satisfies  $\phi(J_i J_i^T) \approx 1$  and  $\lambda \in \mathbb{N}^+ < L$ .*

*Proof.* It is detailed in **Supplementary Material A**.  $\square$

In a nutshell, we find that  $LIF(\cdot)$  is not qualified as a serial function between blocks for achieving block dynamical isometry, which may manifest itself as the degradation problem. However, MS-ResNet can avoid this drawback and attain great stability constituting a much shallower network in effect than it appears to be for gradient norm.

## 4.3 Spike-based Convolution

It should be pointed out that ResNet without interblock  $LIF(\cdot)$  is also undesired for SNNs. One main source of energy efficiency for neuromorphic computing is the spike-based convolution, which means that convolutional layers will receive and process binary spiking input and it is feasible to replace multiply-and-accumulate (MAC) operations

in ANNs with spike-driven synaptic accumulate (AC) operations in SNNs. Once interblock  $LIF(\cdot)$  is removed, the CONV at the top of the next block will receive the continuous input rather than binary spikes, causing difficulty in benefiting from spike-based convolution and rich input/output sparsity.

In addition, removing the interblock  $LIF(\cdot)$  will, in effect, make the convolutional layer in the residual path connected with the one at the top of its subsequent block, and weaken their feature extraction ability. It turns out that the accuracy of W/O  $LIF(\cdot)$  will be lower than the vanilla model before the degradation problem occurs (Table 2). Therefore, we place an extra  $LIF(\cdot)$  at the top of the residual path in order to maintain spike-based convolution as well as fully utilize the convolutional layers.

## 4.4 Depth Analysis on CIFAR-10

We carry out the depth analysis experiment on CIFAR-10 with MS-ResNet as well. The results are shown in Table 2, which indicate that our MS-ResNet can expand to a large scale without facing the degradation problem while preserving its accuracy in shallow structures. Besides, we set  $n$  to 36, 80 to obtain extremely deep MS-ResNet110, MS-ResNet482 on CIFAR-10 with test accuracy of 91.7% and 91.9% respectively. Although the improvement in accuracy is not significant due to increasingly prominent overfitting problem (the regularization method in this experiment maintains the same), it surely evidences the scalability and the capability of our model to avoid degradation.

## 5 Experiments

### 5.1 ImageNet

**Experimental Setup.** We evaluate our models on the ImageNet 2012 dataset [Deng *et al.*, 2009]. The models are trained with the 1.28 million training images and tested with the 50k validation images. The training recipe at first simply follows that of He *et al.* for MS-ResNet18 and MS-ResNet34. However, we find MS-ResNet104 would suffer from severe overfitting. Despite accuracy improvement on the validation set, its training accuracy improves by a significantly larger margin. We hypothesize that it is because MS-ResNet104 has much higher model capacity. To fully unleash the potential of the deep spiking model MS-ResNet104, an advanced training recipe is taken with stronger data augmentation and stronger regularization (See **Supplementary Material B** for more details).

**Results.** As the network deepens, a satisfying tendency of accuracy increase has been observed (Table 3). It evidences the scalability of our models and clearly demonstrates the potential of deepening SNN models. When compared with other advanced works, MS-ResNet34 with an accuracy of **69.42%** surpasses all previous directly trained SNNs at the same depth, and MS-ResNet104 with an accuracy of **74.21%** is even comparable to the converted SNNs in spite of much fewer time steps required for an inference. We also find that just enlarging the images for inference from  $224 \times 224$  to  $288 \times 288$  can improve the accuracy to a more competitive score at 76.02%.

Method	Work	Model	Time step	Acc. (%)	
ANN Conversion	[Sengupta <i>et al.</i> , 2019]	VGG-16	2500	69.96	
		ResNet-34		65.47	
	[Han <i>et al.</i> , 2020]	VGG-16	4096	73.09	
		ResNet-34		69.89	
	[Hu <i>et al.</i> , 2018]	ResNet-34	350	71.61	
	[Stöckl and Maass, 2021] <sup>†</sup>	ResNet-50	500	72.75	
Direct Training		ResNet-50		75.10	
	[Zheng <i>et al.</i> , 2021]	EfficientNet-B7	3488	83.57	
		ResNet-50	6	64.88	
	[Fang <i>et al.</i> , 2021]	Wide-ResNet-34		67.05	
Direct Training		ResNet-34	4	67.04	
		ResNet-101		68.76	
	Our Work MS-ResNet	ResNet-18	6	63.10	
		ResNet-34		69.42	
Backpropagation		ResNet-104	5	74.21	
		ResNet-104*		76.02	
		ResNet-18		69.76	
ANN	ResNet-34	/	73.30		
	ResNet-104 <sup>‡</sup>		76.87		

Table 3: ImageNet results. <sup>†</sup>A spike is allowed to carry multi-bit information. <sup>‡</sup>Since ResNet-104 is not a standard ResNet model, we train its ANN counterpart under the same recipe. \*The input crops are enlarged to 288×288 in inference.

Work	Method	Params	Acc. (%)
[Ramesh <i>et al.</i> , 2020]	DART	N.A.	65.78
[Kugele <i>et al.</i> , 2020]	Rollout-ANN	0.5M	66.75
[Zheng <i>et al.</i> , 2021]	Spiking ResNet-19	12.6M	67.80
[Yao <i>et al.</i> , 2021]	TA-SNN	1.7M	72.00
[Fang <i>et al.</i> , 2020]	PLIF	1.5M	74.80
<b>Our work</b>	<b>MS-ResNet20</b>	0.27M	<b>75.56</b>

Table 4: Results on CIFAR10-DVS.

## 5.2 CIFAR10-DVS

**Experimental Setup.** CIFAR10-DVS is an event-stream dataset for object classification [Li *et al.*, 2017]. 10,000 frame-based images from CIFAR-10 are recorded by a dynamic vision sensor (DVS) and converted into event streams. We take the dataset to test our models for their capability of spatiotemporal processing.

**Results.** MS-ResNet20 achieves a new record on CIFAR10-DVS (Table 4). The model mainly follows the paradigm in Table 1 except that an additional downsampling is placed at the first convolution stage due to larger input size. Our model, despite its depth, actually has a smaller amount of parameters, which is about one-sixth of those in Yao *et al.* and Fang *et al.*.

## 5.3 Energy Efficiency Estimation

Great sparsity is observed in MS-ResNet. The firing rates of MS-ResNet34 and MS-ResNet104, defined as the firing probability of each neuron per time step, are **0.225** and **0.192**, respectively. We also estimate the energy cost based on the number of operations and the data for various operations in 45nm technology [Horowitz, 2014]. We mainly focus on the

Model	32bit-FP:		MAC	4.6pJ	AC	0.9pJ
	G-FLOPs	E(ANN) (1E-3J)	G-SyOPs	E(SNN) (1E-3J)		
ResNet-34	3.53		16.22		4.77	4.29
ResNet-104	11.79		54.24		11.32	10.19

Table 5: Energy consumption for a single ImageNet image.

convolutional layers in residual paths, which constitute a major part of floating-point operations (FLOPs). With the sparsity of spikes and short simulation process, MS-ResNet can achieve the calculation with about the same number of synaptic operations (SyOPs) rather than FLOPs (Table 5), which means that **each neuron emits only one spike on average**. For a single ImageNet image, the energy cost in an SNN are a third to a fifth of that in the ANN with the same structure, and for each frame of CIFAR10-DVS, it is one twenty-fourth (see **Supplementary material C**).

## 6 Conclusion

In this work, we propose a novel spiking residual block to tackle the degradation problem, which enables the direct training of a 482-layer model on CIFAR-10 and a 104-layer model on ImageNet. The great depth brings superior representation power. To our best knowledge, this is the first time such high performance is reported on ImageNet with directly trained SNNs. In addition, our resulting models attain very sparse spiking activities and extremely short simulation, indicating remarkable energy efficiency especially for spatiotemporal information processing. We believe a deep and powerful SNN model is surely to work as the backbone for further exploration in brain-inspired computing.

## A Gradient Evolvement at Backpropagation

### A.1 Proof of Proposition 1

**Lemma A.1** (Multiplication). (*Theorem 4.1 in Chen et al.*) Given  $\mathbf{J} := \prod_{i=L}^1 \mathbf{J}_i$ , where  $\{\mathbf{J}_i \in \mathbb{R}^{m_i \times m_{i-1}}\}$  is a series of independent random matrices. If  $(\prod_{i=L}^1 \mathbf{J}_i)(\prod_{i=L}^1 \mathbf{J}_i)^T$  is at least the 1<sup>st</sup> moment unitarily invariant, we have

$$\phi \left( \left( \prod_{i=L}^1 \mathbf{J}_i \right) \left( \prod_{i=L}^1 \mathbf{J}_i \right)^T \right) = \prod_{i=L}^1 \phi(\mathbf{J}_i \mathbf{J}_i^T). \quad (11)$$

**Lemma A.2** (Addition). (*Theorem 4.2 in Chen et al.*) Given  $\mathbf{J} := \prod_{i=L}^1 \mathbf{J}_i$ , where  $\{\mathbf{J}_i \in \mathbb{R}^{m_i \times m_{i-1}}\}$  is a series of independent random matrices. If at most one matrix in  $\mathbf{J}_i$  is not a central matrix, we have

$$\phi(\mathbf{J} \mathbf{J}^T) = \sum_i \phi(\mathbf{J}_i \mathbf{J}_i^T). \quad (12)$$

**Proposition A.1.** Assuming both two neural networks consisting of  $L$  sequential blocks, the vanilla spiking ResNet does not achieve block dynamical isometry while MS-ResNet could be as stable as a  $\lambda$ -layer network which satisfies  $\phi(\mathbf{J}_i \mathbf{J}_i^T) \approx 1$  and  $\lambda \in \mathbb{N}^+ < L$ .

*Proof.* According to Lemma A.1, the Jacobian matrix of the whole network can be decomposed into the multiplication of its blocks' Jacobian matrices. The gate function within  $LIF(\cdot)$  is defined as:  $g(x) = \begin{cases} 1, & x - V_{th} \geq 0 \\ 0, & x - V_{th} < 0 \end{cases}$  with its surrogate gradient  $g'(x) = \frac{1}{a} \text{sign}(|x - V_{th}| \leq \frac{a}{2})$ , so the Jacobian matrix  $\mathbf{J}_g$  is a diagonal matrix whose elements are either 0 or  $\frac{1}{a}$ . The probability density function  $\rho_{\mathbf{J}_g}(z) = (1-p)\delta(z) + p\delta(z - \frac{1}{a})$ , where  $p$  denotes the probability that  $(x - V_{th}) \leq \frac{a}{2}$  is true. Thus we have

$$\begin{aligned} \phi(\mathbf{J}_g \mathbf{J}_g^T) &= \int_{\mathbb{R}} z((1-p)\delta(z) + p\delta(z - \frac{1}{a^2})) dz = \frac{p}{a^2}, \\ \varphi(\mathbf{J}_g \mathbf{J}_g^T) &= \int_{\mathbb{R}} z^2((1-p)\delta(z) + p\delta(z - \frac{1}{a^2})) dz - \phi(\mathbf{J}_g \mathbf{J}_g^T)^2 \\ &= \frac{p - p^2}{a^4}. \end{aligned} \quad (13)$$

$a$  is a fixed global hyper-parameter so it is difficult to match with the dynamic probability  $p$  between different layers. In addition, even if we assume  $p = a^2$  so that  $\phi(\mathbf{J}_g \mathbf{J}_g^T) = 1$  can hold,  $\varphi(\mathbf{J}_g \mathbf{J}_g^T) = \frac{1}{p} - 1$  can not approximate 0 due to the sparsity of firing activity in SNNs. Therefore, the gate function makes  $LIF(\cdot)$  not qualified as a serial block for Definition 1, which indicates the gradient flow of vanilla spiking ResNet is not stable and may manifest itself as the degradation problem.

While for MS-ResNet, if we denote the Jacobian matrix of the residual path in a block as  $\widetilde{\mathbf{J}_i}$ , according to Lemma A.2 we have  $\phi(\mathbf{J}_i \mathbf{J}_i^T) = 1 + \gamma^2 \phi(\widetilde{\mathbf{J}_i} \widetilde{\mathbf{J}_i}^T)$ , where  $\gamma$  is from the linear scale transformation  $\gamma x + \beta$  within the normalization at the bottom of a residual path. MS-ResNet can be viewed as

an extreme example of Lemma 1 with  $(1 - \omega) \rightarrow 0$ . Therefore  $\forall \lambda$ ,  $C_L^\lambda (1 - \omega)^\lambda$  is close to zero, and  $C_L^\lambda \gamma^\lambda$  can be small enough for a given  $\lambda$  if  $\gamma$  is initialized as a relative small value. In this way, the error of non-optimal block will be influential only within  $\lambda$  layers and the MS-ResNet will be as stable as a much shallower  $\lambda$ -layer network.  $\square$

## B Experimental Details

### B.1 Neuronal Configuration

Parameter configuration about the LIF neuron model is shown in Table 6, and it is kept in all experiments of this work.

Parameter	Value
$V_{th}$	0.5
$V_{reset}$	0
$\tau_{mem}$	0.25
$a$	1

Table 6: Parameter configurations for the LIF neuron model in all experiments.

### B.2 CIFAR-10 Training Details

By setting  $n$  to 5, 7, 9, 18, 80 in Table 7, we obtain our spiking ResNet-32,44,56,110,482. In the experiments of depth analysis, the models are all trained under a simple training recipe, which includes a total of 100 training epochs using an SGD optimizer with 1e-4 L2-penalty and a cosine annealing learning rate scheduler [Loshchilov and Hutter, 2016]. The batchsize is set to 100 and the initial learning rate is 0.1. The experiment is conducted on no more than two NVIDIA RTX 2080Ti GPUs, depending on the memory cost. Synchronized BN technique will be used if multiple GPUs are required. We report the average test accuracy of the last five epochs as our results.

Layers	1 + 2n	2n	2n
Output size	32x32	16x16	8x8
Channels	16	32	64

Table 7: The structure for depth analysis on CIFAR-10.

In Figure 3 we show the training curves of models with varying depths on CIFAR-10 [Krizhevsky *et al.*, 2009]. As the model deepens, the representation power gradually increases, resulting in stable improvement on the training set. The degradation problem is avoided even at a depth of 482 layers. However due to the simple regularization technique we adopt, the overfitting problem has grown more prominent and the impact of the depth on test accuracy is weakened.

### B.3 ImageNet Training Details

For the experiments on ImageNet [Deng *et al.*, 2009], we mainly follow the architectures of the canonical ResNet as in Table 8, but the original MaxPool after the stage of Conv1

Stage	Output Size	ResNet-18	ResNet-34	ResNet-104
Conv1	112x112	7x7, 64, stride=2		
Conv2	56x56	$\begin{bmatrix} 3x3, 64 \\ 3x3, 64 \end{bmatrix} * 2$	$\begin{bmatrix} 3x3, 64 \\ 3x3, 64 \end{bmatrix} * 3$	$\begin{bmatrix} 3x3, 64 \\ 3x3, 64 \end{bmatrix} * 3$
Conv3	28x28	$\begin{bmatrix} 3x3, 64 \\ 3x3, 64 \end{bmatrix} * 2$	$\begin{bmatrix} 3x3, 64 \\ 3x3, 64 \end{bmatrix} * 4$	$\begin{bmatrix} 3x3, 64 \\ 3x3, 64 \end{bmatrix} * 8$
Conv4	14x14	$\begin{bmatrix} 3x3, 64 \\ 3x3, 64 \end{bmatrix} * 2$	$\begin{bmatrix} 3x3, 64 \\ 3x3, 64 \end{bmatrix} * 6$	$\begin{bmatrix} 3x3, 64 \\ 3x3, 64 \end{bmatrix} * 32$
Conv5	7x7	$\begin{bmatrix} 3x3, 64 \\ 3x3, 64 \end{bmatrix} * 2$	$\begin{bmatrix} 3x3, 64 \\ 3x3, 64 \end{bmatrix} * 3$	$\begin{bmatrix} 3x3, 64 \\ 3x3, 64 \end{bmatrix} * 8$
FC	1x1	AveragePool, FC-1000		

Table 8: Structures for ImageNet.

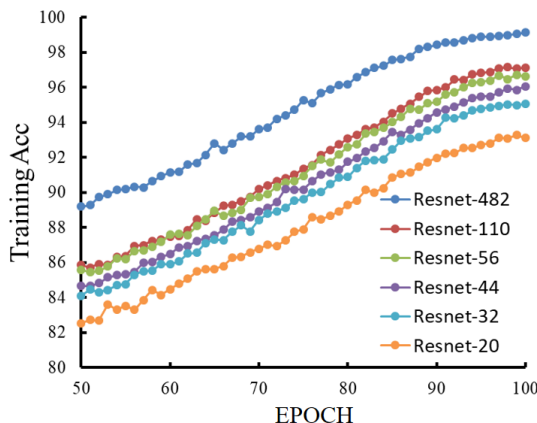


Figure 3: Training curves on CIFAR-10.

is replaced by a stride-2 convolution at the beginning of the Conv2 stage.

The training recipe at first simply follows that of He *et al.* for MS-ResNet18 and MS-ResNet34, i.e., a 224x224 random crop with horizontal flip for data augmentation and an SGD optimizer with a weight decay of 1e-4 and a momentum of 0.9. The training contains 125 epochs and the initial learning rate linearly increases by 0.1 for every 256 batchsize. We report the average test accuracy of the last five epochs as our results.

Unfortunately, we observe severe overfitting problem when extending the model to 104-layer deep. An accuracy increase of 15% on the training set only leads to an increase of 0.5% on the test set. Therefore, a more advanced training recipe is adopted to fully unleash the potential of the deep model.

For the training of MS-ResNet104, we use AutoAugment [Cubuk *et al.*, 2019] for stronger data augmentation, adopt label smoothing [Szegedy *et al.*, 2016] and dropout [Krizhevsky *et al.*, 2017] before the fully-connected layer for stronger regularization. Besides, a 2x2 average pooling layer with a stride of 2 is added before each stride-2-Conv1x1 in the shortcut connection for downsampling, and

the stride of the Conv1x1 is changed to 1 in order not to discard information [He *et al.*, 2019].

A longer training procedure is expected to cooperate with the above techniques, but the direct training of SNNs requires time-consuming backpropagation through time. For saving training time, we propose a two-phase training consisting of a T=1 pre-train phase and a formal training phase. The model is limited to one single time step and gets trained for 200 epochs with large batchsize and learning rate, which is set to 0.1 per 256 batchsize. Then the pre-trained model is utilized as a basis for further learning of temporal dynamics and efficient multi-timesteps expression. The fine-tune phase contains another 100 epochs and the model is trained with 1e-5 L2-penalty and the learning rate is set to 0.05 per 256 batch-size. The pre-train phase only occupies one-ten of the total training time. It is shown in Table 9 that the T=1 pre-trained model can provide a good starting point, and the additional fine-tune phase further accommodates the model to effective spatiotemporal expression.

The number of time steps  $T$  is set to 6 for training. In ResNet-104, however, we find that setting  $T$  to 5 for only inference will cause no harm to the performance, so it is adopted in our final accuracy results and energy estimation.

Depth	T=1	T=6	T=6
	Pre-train	Extended	Fine-tune
34	64.92	66.7	69.5
104	71.72	72.8	74.21

Table 9: The results of pre-train, directly extending T for only inference, and fine-tune formal training.

The BN layer performs a linear scale transformation after standardizing its input  $\gamma\hat{x} + \beta$ . We notice that initializing  $\gamma$  to zero at the end of a residual block will give the model a clean and branch-less starting point and provide a faster convergence, which is also observed in ANNs [He *et al.*, 2019].

The experiment is conducted on up to 8 NVIDIA RTX 2080Ti GPUs, depending on the memory cost. Synchronized

BN technique will be used if multiple GPUs are required.

## C Energy Estimation for CIFAR10-DVS

When dealing with spatiotemporal stream data, ANNs are expected to possess an ability of sequence processing, and consequently recurrent connections are introduced for memorizing previous states and behaving temporal dynamics [He *et al.*, 2020]. Different from the process of a static image, both ANNs and SNNs will spend multiple time steps to perform frame-based information integral for tasks of sequence learning. The conversion method is inherently inappropriate for the rapid process of time-varying input, because it takes time for the firing rates to converge to their targets derived from the pre-trained ANN model [Kugele *et al.*, 2020].

FLOPs	E(ANN) (1E-6J)	SyOPs	E(SNN) (1E-6J)	$\frac{E(ANN)}{E(SNN)}$
40.11M	184.46	8.32M	7.49	24.63

Table 10: Convolutional energy consumption per frame of CIFAR10-DVS.

We assume the ANN has an identical spatial structure of information aggregation as our MS-ResNet20 and make an operation-based energy consumption based on the data from Horowitz. The average firing rate of our MS-ResNet20 model is 22.19% for CIFAR10-DVS [Li *et al.*, 2017]. With the binary and sparse spiking activity, the energy consumption of processing each frame of CIFAR10-DVS in SNNs is one twenty-fourth of that in ANNs (Table 10).

## References

[Chen *et al.*, 2020] Zhaodong Chen, Lei Deng, Bangyan Wang, Guoqi Li, and Yuan Xie. A comprehensive and modularized statistical framework for gradient norm equality in deep neural networks. *IEEE Transactions on Pattern Analysis and Machine Intelligence*, 2020.

[Cubuk *et al.*, 2019] Ekin D. Cubuk, Barret Zoph, Dandelion Mane, Vijay Vasudevan, and Quoc V. Le. Autoaugment: Learning augmentation strategies from data. In *Proceedings of the IEEE/CVF Conference on Computer Vision and Pattern Recognition (CVPR)*, June 2019.

[Deng *et al.*, 2009] Jia Deng, Wei Dong, Richard Socher, Li-Jia Li, Kai Li, and Li Fei-Fei. Imagenet: A large-scale hierarchical image database. In *2009 IEEE Conference on Computer Vision and Pattern Recognition*, pages 248–255, 2009.

[Fang *et al.*, 2020] Wei Fang, Zhaofei Yu, Yanqi Chen, Timothee Masquelier, Tiejun Huang, and Yonghong Tian. Incorporating learnable membrane time constant to enhance learning of spiking neural networks, 2020.

[Fang *et al.*, 2021] Wei Fang, Zhaofei Yu, Yanqi Chen, Tiejun Huang, Timothée Masquelier, and Yonghong Tian. Deep residual learning in spiking neural networks, 2021.

[Han *et al.*, 2020] Bing Han, Gopalakrishnan Srinivasan, and Kaushik Roy. Rmp-snn: Residual membrane potential neuron for enabling deeper high-accuracy and low-latency spiking neural network. In *Proceedings of the IEEE/CVF Conference on Computer Vision and Pattern Recognition (CVPR)*, June 2020.

[He *et al.*, 2016a] Kaiming He, Xiangyu Zhang, Shaoqing Ren, and Jian Sun. Deep residual learning for image recognition. In *Proceedings of the IEEE Conference on Computer Vision and Pattern Recognition (CVPR)*, June 2016.

[He *et al.*, 2016b] Kaiming He, Xiangyu Zhang, Shaoqing Ren, and Jian Sun. Identity mappings in deep residual networks. In Bastian Leibe, Jiri Matas, Nicu Sebe, and Max Welling, editors, *Computer Vision – ECCV 2016*, pages 630–645, Cham, 2016. Springer International Publishing.

[He *et al.*, 2019] Tong He, Zhi Zhang, Hang Zhang, Zhongyue Zhang, Junyuan Xie, and Mu Li. Bag of tricks for image classification with convolutional neural networks. In *Proceedings of the IEEE/CVF Conference on Computer Vision and Pattern Recognition (CVPR)*, June 2019.

[He *et al.*, 2020] Weihua He, YuJie Wu, Lei Deng, Guoqi Li, Haoyu Wang, Yang Tian, Wei Ding, Wenhui Wang, and Yuan Xie. Comparing snns and rnns on neuromorphic vision datasets: Similarities and differences. *Neural Networks*, 132:108–120, 2020.

[Horowitz, 2014] Mark Horowitz. 1.1 computing’s energy problem (and what we can do about it). In *2014 IEEE International Solid-State Circuits Conference Digest of Technical Papers (ISSCC)*, pages 10–14, 2014.

[Hu *et al.*, 2018] Yangfan Hu, Huajin Tang, and Gang Pan. Spiking deep residual network. *arXiv preprint arXiv:1805.01352*, 2018.

[Krizhevsky *et al.*, 2009] Alex Krizhevsky, Geoffrey Hinton, et al. Learning multiple layers of features from tiny images. 2009.

[Krizhevsky *et al.*, 2017] Alex Krizhevsky, Ilya Sutskever, and Geoffrey E. Hinton. Imagenet classification with deep convolutional neural networks. *Commun. ACM*, 60(6):84–90, May 2017.

[Kugele *et al.*, 2020] Alexander Kugele, Thomas Pfeil, Michael Pfeiffer, and Elisabetta Chicca. Efficient processing of spatio-temporal data streams with spiking neural networks. *Frontiers in Neuroscience*, 14:439, 2020.

[Li *et al.*, 2017] Hongmin Li, Hanchao Liu, Xiangyang Ji, Guoqi Li, and Luping Shi. Cifar10-dvs: An event-stream dataset for object classification. *Frontiers in Neuroscience*, 11:309, 2017.

[Loshchilov and Hutter, 2016] Ilya Loshchilov and Frank Hutter. SGDR: Stochastic Gradient Descent with Warm Restarts. *arXiv e-prints*, page arXiv:1608.03983, August 2016.

[Maass, 1997] Wolfgang Maass. Networks of spiking neurons: The third generation of neural network models. *Neural Networks*, 10(9):1659–1671, 1997.

[Neftci *et al.*, 2019] Emre O. Neftci, Hesham Mostafa, and Friedemann Zenke. Surrogate gradient learning in spiking neural networks: Bringing the power of gradient-based optimization to spiking neural networks. *IEEE Signal Processing Magazine*, 36(6):51–63, 2019.

[Ramesh *et al.*, 2020] Bharath Ramesh, Hong Yang, Garrick Or- chard, Ngoc Anh Le Thi, Shihao Zhang, and Cheng Xiang. Dart: Distribution aware retinal transform for event-based cameras. *IEEE Transactions on Pattern Analysis and Machine Intelligence*, 42(11):2767–2780, 2020.

[Roy *et al.*, 2019] Kaushik Roy, Akhilesh Jaiswal, and Priyadarshini Panda. Towards spike-based machine intelligence with neuromorphic computing. *Nature*, 575(7784):607–617, 2019.

[Rueckauer *et al.*, 2017] Bodo Rueckauer, Iulia-Alexandra Lungu, Yuhuang Hu, Michael Pfeiffer, and Shih-Chii Liu. Conversion of continuous-valued deep networks to efficient event-driven

networks for image classification. *Frontiers in Neuroscience*, 11:682, 2017.

[Sengupta *et al.*, 2019] Abhroni Sengupta, Yuting Ye, Robert Wang, Chiao Liu, and Kaushik Roy. Going deeper in spiking neural networks: Vgg and residual architectures. *Frontiers in Neuroscience*, 13:95, 2019.

[Srivastava *et al.*, 2015] Rupesh Kumar Srivastava, Klaus Greff, and Jürgen Schmidhuber. Training very deep networks. In *Proceedings of the 28th International Conference on Neural Information Processing Systems - Volume 2*, NIPS’15, page 2377–2385, Cambridge, MA, USA, 2015. MIT Press.

[Stöckl and Maass, 2021] Christoph Stöckl and Wolfgang Maass. Optimized spiking neurons can classify images with high accuracy through temporal coding with two spikes. *Nature Machine Intelligence*, 3(3):230–238, 2021.

[Szegedy *et al.*, 2015] Christian Szegedy, Wei Liu, Yangqing Jia, Pierre Sermanet, Scott Reed, Dragomir Anguelov, Dumitru Erhan, Vincent Vanhoucke, and Andrew Rabinovich. Going deeper with convolutions. In *Proceedings of the IEEE Conference on Computer Vision and Pattern Recognition (CVPR)*, June 2015.

[Szegedy *et al.*, 2016] Christian Szegedy, Vincent Vanhoucke, Sergey Ioffe, Jon Shlens, and Zbigniew Wojna. Rethinking the inception architecture for computer vision. In *Proceedings of the IEEE Conference on Computer Vision and Pattern Recognition (CVPR)*, June 2016.

[Tarnowski *et al.*, 2019] Wojciech Tarnowski, Piotr Warchał, Stanisław Jastrzębski, Jacek Tabor, and Maciej Nowak. Dynamical isometry is achieved in residual networks in a universal way for any activation function. In Kamalika Chaudhuri and Masashi Sugiyama, editors, *Proceedings of the Twenty-Second International Conference on Artificial Intelligence and Statistics*, volume 89 of *Proceedings of Machine Learning Research*, pages 2221–2230. PMLR, 16–18 Apr 2019.

[Veit *et al.*, 2016] Andreas Veit, Michael Wilber, and Serge Belongie. Residual networks behave like ensembles of relatively shallow networks. In *Proceedings of the 30th International Conference on Neural Information Processing Systems*, NIPS’16, page 550–558, Red Hook, NY, USA, 2016. Curran Associates Inc.

[Wu *et al.*, 2019] Yujie Wu, Lei Deng, Guoqi Li, Jun Zhu, Yuan Xie, and Luping Shi. Direct training for spiking neural networks: Faster, larger, better. *Proceedings of the AAAI Conference on Artificial Intelligence*, 33(01):1311–1318, Jul. 2019.

[Yao *et al.*, 2021] Man Yao, Huanhuan Gao, Guangshe Zhao, Dingheng Wang, Yihan Lin, Zhaoxu Yang, and Guoqi Li. Temporal-wise attention spiking neural networks for event streams classification. *arXiv preprint arXiv:2107.11711*, 2021.

[Zheng *et al.*, 2021] Hanle Zheng, Yujie Wu, Lei Deng, Yifan Hu, and Guoqi Li. Going deeper with directly-trained larger spiking neural networks. *Proceedings of the AAAI Conference on Artificial Intelligence*, 35(12):11062–11070, May 2021.